Blind Transmitter IQ Imbalance Compensation in *M*-QAM Optical Coherent Systems

Trung-Hien Nguyen, Pascal Scalart, Mathilde Gay, Laurent Bramerie, Olivier Sentieys, Jean-Claude Simon, Christophe Peucheret, and Michel Joindot

***Abstract*—We investigate transmitter IQ imbalance compensation based on the blind adaptive source separation (BASS) method in a dual-polarization *M*-QAM optical coherent system. The robustness of the BASS method against the residual carrier frequency offset (CFO) is numerically investigated and compared to that of the Gram–Schmidt orthogonalization procedure (GSOP). We further validate experimentally the proposed method with 10 Gbaud optical 4-QAM and 16-QAM signals at 30° and 10° phase imbalance, respectively, with simulated impairments. More specifically, in the presence of 5×10^{-6} residual CFO (normalized to the sample rate), the optical signal-to-noise ratio penalty reduction of the BASS method compared to the GSOP method is 1 dB for 4-QAM at a bit error ratio (BER) of 2×10^{-3} and 2 dB for 16-QAM at a BER of 10^{-3}. In contrast to the GSOP, which requires an independent block, the BASS method can be integrated into an equalizer, simplifying the operation and allowing parallel implementation.**

***Index Terms*—Digital signal processing; IQ imbalance compensation; *M*-QAM; Optical coherent transmission.**

I. Introduction

M-ary quadrature amplitude modulation (*M*-QAM) in combination with coherent detection and digital signal processing (DSP) has now become a promising candidate for next-generation optical transmission systems. This is made possible notably thanks to technical progress in photonic integrated circuits (PICs) allowing the fabrication of monolithically integrated optical circuits for *M*-QAM optical signal generation [1]. Despite the amazing performance of these circuits, there are still some issues, in particular concerning the nonlinear gain of electrical amplifiers, the control of phase shifts in optical waveguides, and the cable lengths or circuit paths on printed boards. For all these reasons the resulting signal may present gain and/or phase imbalance, globally referred to as IQ imbalance.

As the modulation order increases, the sensitivity to such imperfections is exacerbated, especially under the impacts of carrier frequency offset (CFO) between the transmitter (Tx) laser and receiver (Rx), chromatic dispersion (CD), and polarization-multiplexing-induced effects. Some effort has been dedicated to Rx IQ imbalance compensation with the help of DSP, including the Gram–Schmidt orthogonalization procedure (GSOP) [2] or complex-valued multiple-input-multiple-output (MIMO) adaptive equalizers [3,4]. A widely linear equalizer has recently been studied for joint Rx IQ imbalance compensation and polarization demultiplexing [5]. Tx IQ imbalance is more critical in transmission systems, and some recent work has attempted to eliminate this impairment, e.g., by using Turbo demodulation of LDPC-coded signals [6] or indirect learning architecture [7] as a calibration method, regardless of transmission imperfections, such as CD and polarization-multiplexing-induced impairments. Tx IQ imbalance monitoring and diagnosis functions based on adaptive filter coefficients have recently been proposed in [8]. However, an extra 2×2 MIMO filter is required for each polarization, implying increased hardware complexity. Table I presents a comparison of existing IQ imbalance compensation methods in terms of their implementation, validation, complexity, and possibility of joint compensation of other impairments.

In our recent work [9], we have shown that the CFO should be compensated for before the IQ imbalance compensation in the presence of Tx IQ imbalance. In addition, residual CFO is always present, even when using advanced CFO compensation [10], and it can only be mitigated at the carrier recovery stage (after the polarization demultiplexing filters). In this paper, we extend the use of a blind adaptive source separation (BASS) algorithm in a dual-polarization *M*-QAM optical coherent system in order to compensate for the Tx IQ imbalance. The order of DSP blocks is optimized to reduce the hardware complexity while keeping the effectiveness of the Tx IQ imbalance compensation. To this aim, the equalizer structure is revisited to carry out simultaneous polarization demultiplexing, IQ imbalance, and residual CD compensation. The

Manuscript received January 18, 2017; revised May 1, 2017; accepted June 14, 2017; published August 11, 2017 (Doc. ID 284782).

T.-H. Nguyen (e-mail: trung-hien.nguyen@ulb.ac.be) was with the FOTON Laboratory, CNRS, University of Rennes 1, ENSSAT, F-22305 Lannion, France. He is now with the OPERA Department, Université Libre de Bruxelles, 1050 Ixelles, Belgium.

P. Scalart and O. Sentieys are with INRIA/IRISA, University of Rennes 1, 35000 Rennes, France.

M. Gay, L. Bramerie, J.-C. Simon, C. Peucheret, and M. Joindot are with the FOTON Laboratory, CNRS, University of Rennes 1, ENSSAT, F-22305 Lannion, France.

https://doi.org/10.1364/JOCN.9.000D42

TABLE I
COMPARISON OF EXISTING IQ IMBALANCE COMPENSATION METHODS

Ref.	Polarization	IQ Imbalance Position	Simulation/Experiment	Complexity of Update Rule	Joint/Independent Compensation
[2]	Single	Rx	Simulation	N/A	Independent
[3]	Dual	Rx	Experiment	High	Joint
[4]	Dual	Rx	Simulation	High	Joint
[5]	Dual	Rx	Simulation	High	Joint
[6]	Single	Tx	Simulation	High	Joint
[7]	Single	Tx	Experiment	High	Independent
[8]	Single	Tx	Simulation	High	Independent
[9]	Single	Tx	Both	Medium	Joint
This work	Dual	Tx/Rx (applicable)	Both	Medium	Joint

robustness of the proposed method against residual CFO is investigated and compared to that of the widely used GSOP method. First, a performance comparison between the GSOP and the BASS methods is carried out by extensive simulations with 4-QAM (also known as quadrature phase shift keying—QPSK) and 16-QAM modulations. The results show that our proposed method is more robust against residual CFO, compared to the GSOP. Second, an experimental validation is also carried out with 10 Gbaud optical 4-QAM and 16-QAM signals subjected to 30° and 10° phase imbalance, respectively. In the presence of 5×10^{-6} residual CFO (normalized to the sample rate), our proposed method enables optical signal-to-noise ratio (OSNR) penalty reductions compared to the GSOP method of 1 and 2 dB at bit error ratios (BERs) of 2×10^{-3} and 10^{-3} for the 4-QAM and 16-QAM signals, respectively, showing its effectiveness. Furthermore, while the GSOP method operates based on statistical calculations of collected samples, our proposed method effectively operates at the sample rate, and all proposed DSP blocks work in the feedforward manner. This possibly facilitates parallel implementations and hence is promising for high-bit-rate transmission systems.

The paper is organized as follows: Section II briefly describes a model for Tx IQ imbalance under the impacts of polarization-multiplexing-induced impairments, CD, and CFO. The DSP blocks order and numerical studies of the proposed method are then reported in Section III. The effectiveness of the proposed method is further validated experimentally in Section IV. A comparison of the hardware complexity of the algorithms is summarized in Section V. Finally, Section VI concludes the paper.

II. TX IQ IMBALANCE UNDER THE IMPACT OF TRANSMISSION IMPAIRMENTS

Figure 1 presents a block diagram of a dual-polarization M-QAM coherent transmission system. At the transmitter, the different driving electrical signal amplitudes between the in-phase (I) and quadrature (Q) arms of the modulator and the imperfect biasing are referred to as Tx gain imbalance, ε_p, and phase imbalance, θ_p, respectively [6], where the subscript $p = 1, 2$ denotes polarizations X and Y, respectively. Under the impact of Tx IQ imbalance, the transmitted signal on each polarization, $x_p(t)$, can be expressed as [11]

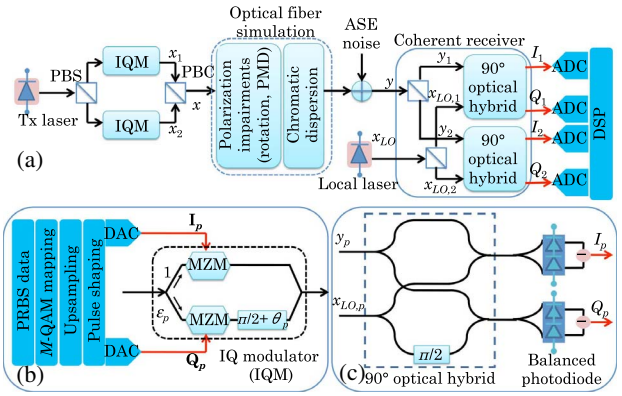

Fig. 1. (a) Block diagram of the dual-polarization M-QAM coherent system under the impacts of Tx IQ imbalance, CFO, CD, and polarization-multiplexing-induced effects. (b) Tx electrical signal generation and IQ modulator structure with IQ imbalance. (c) 90° optical hybrid structure. PBS, polarization beam splitter; PBC, polarization beam combiner.

$$x_p(t) = \Re[s_p(t) \cdot (G_{1,p}e^{j\omega_s t} + G_{2,p}e^{-j\omega_s t})]$$
$$G_{1,p} = (1 + \varepsilon_p e^{j\theta_p})/2, \qquad G_{2,p} = (1 - \varepsilon_p e^{-j\theta_p})/2, \quad (1)$$

where $s_p(t)$ and ω_S denote the baseband signal to be transmitted on the polarization p and the Tx laser frequency, respectively. $(\cdot)^*$ is the complex conjugation operation, $\Re$ is the real-part operator, and $j = \sqrt{-1}$. It should be noted that $G_{1,p} = 1$ and $G_{2,p} = 0$ in the absence of Tx IQ imbalance. Note that the Tx signal is band-limited by a root-raised-cosine (RRC) filter.

The distorted signals are polarization-multiplexed from a single laser source by the polarization beam splitter (PBS) and polarization beam combiner (PBC). The multiplexed signal is then transmitted over a 200-km-long standard single-mode optical fiber (equivalent to an accumulated CD of 3400 ps/nm) [12]. Neglecting the fiber nonlinearity, the transfer function of the transmission medium associated with CD, $H_{\mathrm{CD}}(z, \Delta\omega)$, and with polarization-induced impairments [i.e., polarization mode dispersion (PMD)], $H_{\mathrm{PMD}}(\Delta\omega)$ can be expressed as

$$H(\Delta\omega) = H_{\mathrm{CD}}(z, \Delta\omega)H_{\mathrm{PMD}}(\Delta\omega) \quad (2)$$

where $H_{\mathrm{CD}}(z, \Delta\omega)$ and $H_{\mathrm{PMD}}(\Delta\omega)$ are represented by [13,14]

$$H_{\mathrm{CD}}(z,\Delta\omega)=\exp\left(-j\frac{D\lambda^2 z}{4\pi c}\Delta\omega^2\right), \tag{3}$$

$$H_{\mathrm{PMD}}(\Delta\omega)=\begin{pmatrix}\cos\alpha & \sin\alpha\\ -\sin\alpha & \cos\alpha\end{pmatrix}\begin{pmatrix}e^{j(\Delta\omega\tau+\beta)/2} & 0\\ 0 & e^{-j(\Delta\omega\tau+\beta)/2}\end{pmatrix}\times\begin{pmatrix}\cos\alpha & -\sin\alpha\\ \sin\alpha & \cos\alpha\end{pmatrix},$$

in which z is the propagation distance. The parameters λ and c denote the wavelength and speed of the light in vacuum, respectively. D represents the dispersion coefficient of the fiber. $\Delta\omega$ is the angular frequency with respect to ω_S. The parameters 2α and β are the azimuth angle and elevation angle of the state of polarization in Stokes space. Finally, τ denotes the differential group delay (DGD).

Using this transfer function, the effects of CD, polarization rotation, and PMD can be simulated so that simultaneous polarization demultiplexing and compensation of IQ imbalance and the residual CD and CFO can be verified with the proposed method. After being combined with the signal emitted by a local oscillator (LO) laser, $x_{\mathrm{LO}}(t)$, in a coherent receiver (consisting of two 90° optical hybrid units) and experiencing the effect of CFO, $\omega_0=\omega_L-\omega_S$ (ω_L being the LO laser angular frequency), the received I_p and Q_p components on each polarization after balanced photodetection, can be written as

$$I_p=\Re(y_p\cdot x^*_{\mathrm{LO},p}\cdot e^{-j(\omega_0 t+\varphi(t))})Q_p=\Im(y_p\cdot x^*_{\mathrm{LO},p}\cdot e^{-j(\omega_0 t+\varphi(t))}), \tag{5}$$

in which $y(t)$ is the transmitted signal, corrupted by amplified spontaneous emission (ASE) noise from optical amplifiers and having experienced CD- and polarization-induced impairments. $\Im$ is the imaginary part operator, and $\varphi(t)$ describes the laser phase noise. To simplify our model, we assume that the laser phase noise only comes from the emitter LO laser.

The output signals of the balanced photodiodes are digitized in analog-to-digital converters (ADCs) and subsequently filtered by another RRC filter (acting as a matched filter) to obtain optimal performance. It is assumed that the received signal is sampled at twice the symbol rate and is perfectly time synchronized. The DSP steps are summarized in Fig. 2. They consist of i) CD compensation in the frequency domain [13], ii) frequency-domain-based CFO compensation [10], iii) joint IQ imbalance compensation by the proposed BASS method and polarization demultiplexing filters, iv) phase noise compensation [15], and v) BER and error vector magnitude (EVM) [16] calculations.

Concerning the Tx IQ imbalance compensation step, our proposed BASS method is compared to the GSOP method by simply replacing the BASS method in Fig. 2 by the GSOP method. In fact, IQ imbalance results in an interfering term in the demodulated complex signal that is a linear combination of the useful signal and its complex conjugate

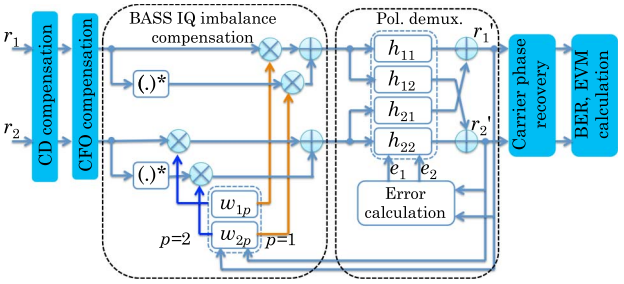

Fig. 2. DSP blocks. The received complex signal is $r_p=I_p+jQ_p$.

version. This relation can be expressed by a matrix [14], and the compensation problem is equivalent to finding the best estimation of the inverse of this matrix in order to recover the useful signal by canceling the interference. This becomes feasible due to the circular property of the signal constellation and due to the fact that $r_p(k)$ and $r_p^*(k)$, in which $r_p(k)=I_p+j\cdot Q_p$, are not correlated so that the statistical expectation $E(r_p^2)=0$ holds [17]. The problem now reduces to the whitening transformation [18] of the received sample blocks and their complex conjugates (which is the key idea behind the BASS method) so that the complex conjugation (induced by IQ imbalance) is eliminated. More specifically, we only need to compute $r'_p(k)=w_{1,p}(k)r_p(k)+w_{2,p}(k)r_p^*(k)$, with $w_{1,p}$ and $w_{2,p}$ being adaptively deduced by [19]

$$\begin{aligned}w_{1,p}(k+1)&=[1-\mu(|r'_p(k)|^2-1)]w_{1,p}(k)-\mu(r'_p(k))^2w^*_{2,p}(k),\\ w_{2,p}(k+1)&=[1-\mu(|r'_p(k)|^2-1)]w_{2,p}(k)-\mu(r'_p(k))^2w^*_{1,p}(k),\end{aligned} \tag{6}$$

where μ is the step-size, and k denotes the index of the kth sample. Note that our algorithm is also modified to be compatible with fractionally spaced equalizers, which further distinguishes this study from the work in [19], which uses symbol-spaced equalizers. Also, the integration of the BASS algorithm with the polarization demultiplexing filter is new. This integration potentially offers reduced complexity compared to the IQ imbalance compensation method in [4]. In order to improve the steady-state performance, we use the radius directed equalization (RDE) instead of the constant modulus algorithm (CMA) -based equalization for polarization demultiplexing [20], especially when high-order modulations, i.e., 16-QAM are considered. The filter coefficients are updated based on the following rules:

$$\begin{aligned}h_{11}(k+1)&=h_{11}(k)+\eta\cdot e_1(k)\cdot(r'_1(k))^*,\\ h_{12}(k+1)&=h_{12}(k)+\eta\cdot e_2(k)\cdot(r'_1(k))^*,\\ h_{21}(k+1)&=h_{21}(k)+\eta\cdot e_1(k)\cdot(r'_2(k))^*,\\ h_{22}(k+1)&=h_{22}(k)+\eta\cdot e_2(k)\cdot(r'_2(k))^*,\end{aligned} \tag{7}$$

where η is the adaptation step-size, and the error criteria $\{e_1(k),e_2(k)\}$ are defined as

$$e_p(k)=r'_p(k)(R_k-|r'_p(k)|^2), \tag{8}$$

in which R_k is the radius of the nearest constellation symbol for each equalizer output [20]. Note that the proposed algorithm is also suitable for Rx IQ imbalance compensation and for both single- and multi-carrier advanced modulation format signals, which is a desirable feature in the context of flexible optical transceivers. It is also worth noticing that in the simulations, the performance upper bound of the IQ imbalance compensation without using the considered compensation methods can be achieved by using the knowledge of $G_{1,p}$ and $G_{2,p}$ after polarization demultiplexing as follows:

$$\hat{r}_p = \frac{(G_{1,p})^* r'_p - G_{2,p}(r'_p)^*}{|G_{1,p}|^2 - |G_{2,p}|^2}. \tag{9}$$

III. Numerical Investigation

To evaluate the performance of the proposed method, the setup in Fig. 1 is numerically simulated for 4-QAM and 16-QAM transmission systems. For all simulations, we assume the symbol rate is 10 Gbaud. At the Tx, pseudo-random binary sequences (PRBSs) with lengths of $2^{23} - 1$ and $2^{15} - 1$ bits are used for generating the signal along polarizations X and Y, respectively. Those sequences are then mapped onto the M-QAM constellations. The QAM symbols are up-sampled to 8 samples per symbol and shaped by the RRC filters with a roll-off factor of 0.5. Their real and imaginary parts are applied to the I and Q inputs of the modulator, respectively, where the Tx IQ imbalance is simulated. To focus on the impact of linear impairments induced by transmission on the Tx IQ imbalance compensation, other nonlinear transmission effects are ignored. The polarization rotation is randomly generated, and the DGD is set to 10 ps. At the Rx, the local laser frequency is set to obtain a CFO of 0.2 GHz (to match typical experimental conditions). The laser linewidth is set to 100 kHz, which is a typical value for commercial external cavity lasers. The received signals are detected by a dual-polarization coherent receiver. To concentrate on the Tx IQ imbalance, the Rx IQ imbalance coming from the imperfection of 90° optical hybrid units is not considered. The resolution of the ADCs is assumed to be sufficiently high to neglect amplitude errors linked to quantization steps. The aforementioned DSPs are applied to the digitized signals. Twenty calculation iterations (with different random noise seeds) are carried out for each IQ imbalance value before averaging the EVM calculations over about 130,000 symbols. Note that a short training sequence, as in e.g., [21], should be used to detect the starting point of the data frame. Based on the training sequence, phase ambiguities can be detected, and initial phase values can be estimated and used as initial values in the subsequent DSP blocks.

The performance is investigated after the convergence of filters using the minimum mean square error criterion. We configure 15 taps for all filters. We assess the performance of the proposed BASS method in comparison to the GSOP method by varying different combinations of IQ gain imbalance (ε_p) and IQ phase imbalance (θ_p) of the two polarizations. The OSNR to achieve a BER of 10^{-3} for each modulation order is considered. However, due to the fact that Tx IQ imbalance compensation always results in OSNR penalties [8], we intentionally add margins of 4 and 9 dB to the required OSNR at the 10^{-3} BER in order to use a large range of IQ imbalance values. Although CFO compensation is required before Tx IQ imbalance compensation [9], some residual CFO is always present in actual situations even if advanced CFO compensation is used [10]. In metro and access networks where the transmission distance is relatively short (≤200 km), residual CFO is expected to be the most detrimental effect on system performance compared to other issues, such as residual CD- or polarization-induced impairments. We therefore focus on the impact of residual CFO in the following study. For the sake of clarity, the residual CFO is normalized to the sample rate and set to 10^{-5} (equivalent to 200 kHz residual CFO in the simulations) if not stated otherwise.

Figure 3 shows the average EVM surface (over two polarizations) as a function of the IQ gain imbalance [Fig. 3(a)] and IQ phase imbalance [Fig. 3(b)] for 4-QAM modulation. For each simulation, when the gain imbalance is varied,

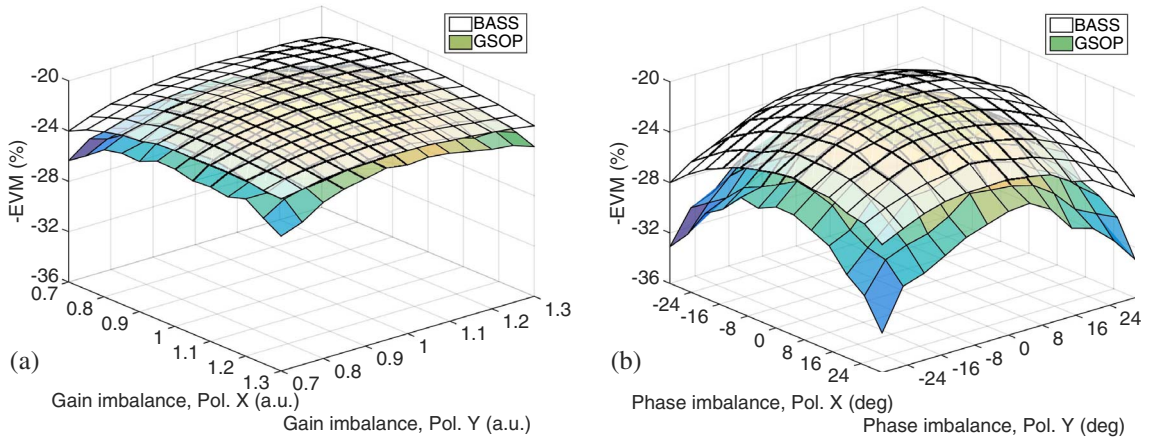

Fig. 3. Average EVM surfaces as a function of the (a) gain imbalance and (b) phase imbalance with 4-QAM modulations. The normalized residual CFO is set to 10^{-5}.

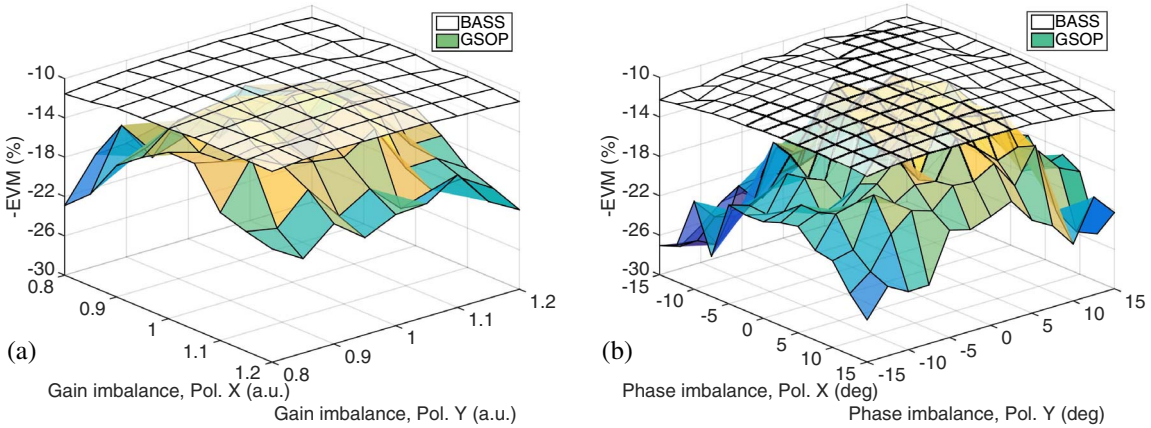

Fig. 4. Average EVM surfaces as a function of the (a) gain imbalance and (b) phase imbalance with 16-QAM modulations. The normalized residual CFO is set to 10^{-5}.

the phase imbalance is not considered and vice versa. It can be seen that the EVM increases with the increase of either gain imbalance or phase imbalance, implying larger distributions of the constellation points away from their ideal positions. The performance degradation caused by the gain imbalance is slower than that caused by the phase imbalance. In all cases, the proposed BASS method is more robust to the residual CFO than the GSOP method. Hence, the BASS method shows better performance than the GSOP method, especially at high values of IQ imbalance. More particularly, the BASS method exhibits about 3% and 5% EVM better than the GSOP method at the respective 0.7 gain imbalance and 30° phase imbalance. Figure 4 presents results of a similar investigation for 16-QAM modulation. Note that the considered imbalance values are smaller than in the case of 4-QAM modulation, since the higher-order modulation format is more sensitive to such impairments. It can be observed that the BASS method still performs properly, while the GSOP method shows poor performance. It can be explained by the fact that the GSOP is less effective in the presence of residual CFO, so the polarization demultiplexing equalizers cannot converge. The RDE for ideal 16-QAM modulation uses three radii for the error criteria [20]. However, the 16-QAM constellation in the presence of residual CFO is spread over more than three radii, making the equalizer unable to converge. The results shown in Figs. 3 and 4 also reveal that the tolerant range of the BASS method within which the IQ imbalance parameters must lie in order to remain within a given performance penalty is much larger than that of the GSOP method, especially in the case of 16-QAM modulations.

Figure 5 presents the convergence speed of the adaptive equalizer for 4- and 16-QAM modulations by calculating the mean square error (MSE) of $e_p(k)/r'_p(k)$ [the modulus difference calculation in Eq. (8)]. In this investigation, the gain and phase imbalance are set to 1.1° and 15°, respectively. The OSNR is fixed to 19 dB, and the BASS algorithm is applied for the IQ imbalance compensation. The MSE calculation is averaged over 100 simulation runs and over two polarizations. It can be observed that the

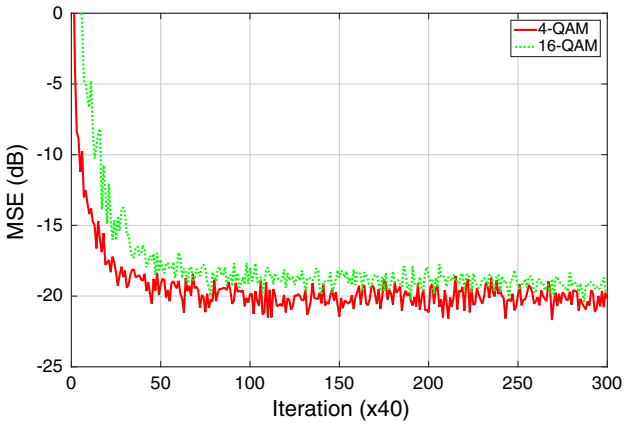

Fig. 5. Convergence speed of the adaptive algorithm using the BASS algorithm for 4- and 16-QAM modulations. The MSE calculation is averaged over two polarizations and over 100 simulation runs.

convergence speed of 4-QAM is better than that of 16-QAM. Under the same impact of the IQ imbalance, the 16-QAM signal is more sensitive to the impairment than the 4-QAM signal, resulting in a slightly higher value of the steady-state convergence.

We further study the impact of a wide-range residual CFO on the performance of dual-polarization 4- and 16-QAM coherent transmission systems. Figures 6 and 7 show the average EVM as a function of the residual CFO for 4- and 16-QAM modulations, respectively. The performance upper bound based on the use of Eq. (9) is plotted as a benchmark for comparison to the performances of the GSOP and BASS methods. In these simulations, for 4-QAM modulation, we fix the gain/phase imbalance values of 1.2°/30° and 1.1°/30° for the polarizations X and Y, respectively. The imbalance values for 16-QAM modulation are equal to 1.1°/10° and 1.05°/10° for the corresponding polarizations X and Y. It can be seen that the EVM becomes worse when a large residual CFO is present. The residual CFO tolerances of the BASS method are 10^{-5} and

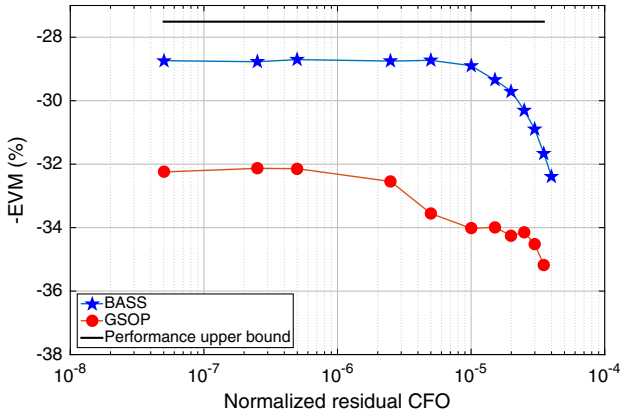

Fig. 6. Average EVM as a function of the normalized residual CFO with 4-QAM modulations. The sets of gain/phase imbalance values of polarizations X and Y are 1.2°/30° and 1.1°/30°, respectively.

3×10^{-6} for 4- and 16-QAM, respectively, before the performance degrades, while that of the GSOP method is about 10^{-6} for both modulations. Note that the performance of the BASS method is always better than that of the GSOP method, even if the residual CFO is small. The proposed method is further validated experimentally with 10 Gbaud 4-QAM and 16-QAM signals in the following study.

IV. Experimental Investigation

The Tx IQ imbalance impact is experimentally investigated for 10 Gbaud 4-QAM and 16-QAM optical coherent systems. Since the effectiveness of the proposed BASS method in a dual-polarization coherent system is numerically demonstrated in the previous section, for the sake of simplification, we consider only one polarization in our experiments. In order to focus on the impact of IQ imbalance and to facilitate tuning the CFO, we simplify the setup in Fig. 1 by using the same laser at the Tx and as the local oscillator (LO) at the Rx, as illustrated in Fig. 8. The

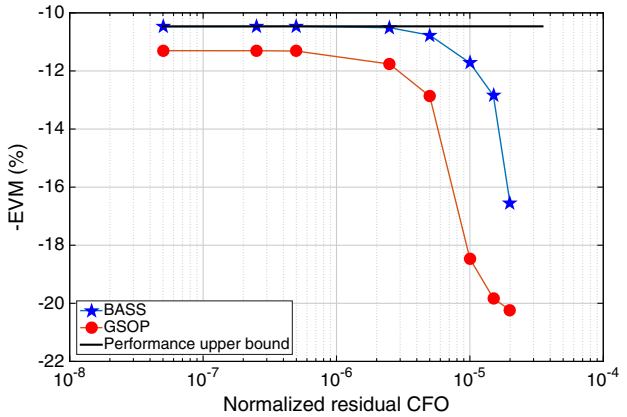

Fig. 7. Average EVM as a function of the normalized residual CFO with 16-QAM modulations. The sets of gain/phase imbalance values of polarizations X and Y are 1.1°/10° and 1.05°/10°, respectively.

estimated linewidth of this optical source is about 100 kHz. At the Tx, 4-QAM and 16-QAM signals are generated in the same way as in simulations with an arbitrary waveform generator (AWG). However, its bandwidth is only 4.8 GHz, which results in inter-symbol interference (ISI) for 10-Gbaud signals. Fortunately, the ISI effect can also be eliminated simultaneously with the other impairments (i.e., residual CD) by the equalizer. Note that the Tx phase imbalance is adjusted by modifying the bias voltage controlling the phase difference between the two arms of the IQ modulator. The Tx IQ gain imbalance is not considered, since it can be easily compensated for by adjusting the gains of the transimpedance amplifiers at the receivers. Moreover, the signal OSNR is varied by using a variable optical attenuator (VOA) cascaded with an erbium-doped fiber amplifier (EDFA) and followed by a 3-nm optical bandpass filter. At the Rx side, an optical 90° hybrid splits and cross combines the M-QAM signal and the LO signal. The I and Q components are detected by balanced photodiodes and acquired by a real-time oscilloscope with an electrical bandwidth of 16 GHz at a rate of 40 GS/s. After data acquisition, DSP is performed offline using the Matlab environment. To emulate the CFO and CD impacts on the IQ imbalance compensation, a CFO of 0.2 GHz and a CD induced by transmission over 200-km standard single-mode fiber are artificially added to the received samples. The CFO compensation is controlled so that the normalized residual CFO is 5×10^{-6}. The BER is calculated over one million samples. Note that DSP is applied to blocks of 200,000 symbols. In the following parts, we experimentally assess the performance of the GSOP and BASS methods in two cases: 1) the back-to-back (B2B) case, corresponding to the case when the transmitter is directly connected to the receiver, without (w/o) CFO and CD impacts, and 2) 200-km transmission with (w/) the previously discussed DSP stages.

Figure 9(a) shows the BER evolution of the 4-QAM signals measured in cases 1 and 2 as a function of the OSNR (with the noise power normalized to a 0.1 nm bandwidth) at a 30° phase imbalance. Note that the phase imbalance value is estimated based on the method in [22]. In case 1, GSOP and BASS exhibit OSNR penalties of 2 and 1.7 dB at a BER of 10^{-3}, respectively, compared to the case when no IQ imbalance is present. In the presence of the emulated CFO and CD (case 2), the effectiveness of the GSOP method is reduced, whereas the BASS method still presents a good IQ imbalance compensation, even though the CFO and CD are not completely compensated for. This is due to the independent operation of BASS in a frequency-selective channel [19]. As a consequence, the BER curve of

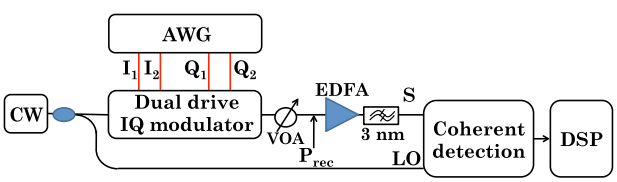

Fig. 8. Experimental setup for the validation of the Tx IQ imbalance compensation.

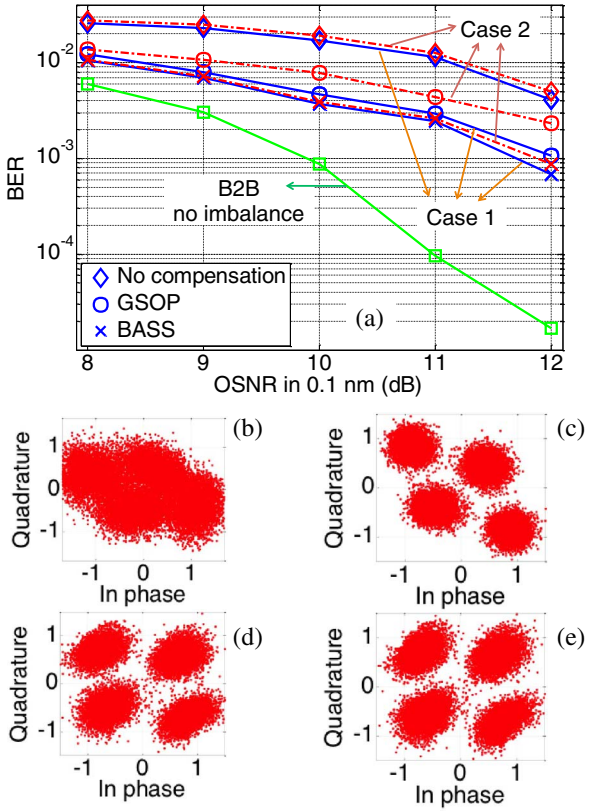

Fig. 9. (a) Evolution of the BER of a 10 Gbaud 4-QAM signal as a function of the OSNR in the presence of 30° phase imbalance (solid lines: case 1; dashed–dotted lines: case 2). Examples of 4-QAM constellations at 10 dB OSNR in the cases of (b) raw data, (c) w/o IQ imbalance compensation, (d) w/GSOP (case 2), and (e) w/BASS (case 2).

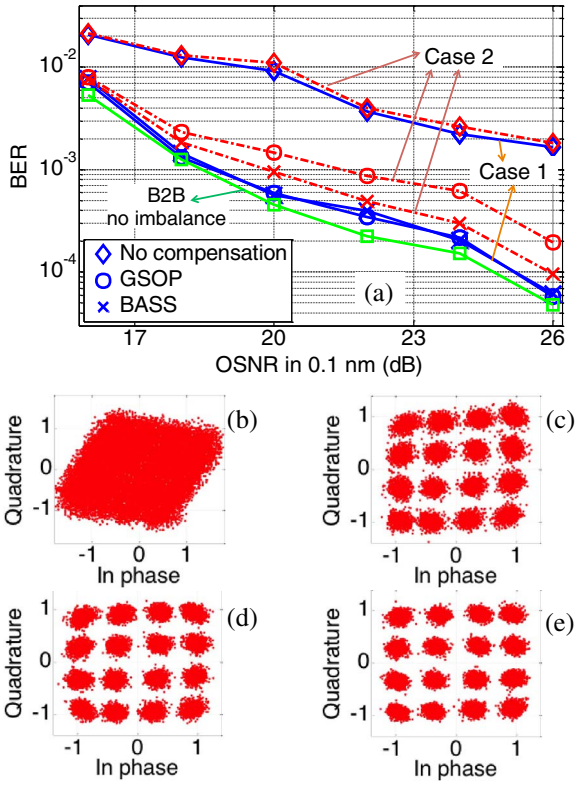

Fig. 10. (a) Evolution of the BER of a 10 Gbaud 16-QAM signal as a function of the OSNR in the presence of 10° phase imbalance (solid lines: case 1; dashed–dotted lines: case 2). Examples of 16-QAM constellations at a 26 dB OSNR in the cases of (b) raw data, (c) w/o IQ imbalance compensation, (d) w/GSOP (case 2), and (e) w/BASS (case 2).

the BASS method in case 2 can be made nearly identical to that in case 1. The BER curve of the GSOP method in case 2 exhibits an OSNR penalty of 1 dB at a BER of 2×10^{-3}, compared to case 1. Note that in case 2, the ISI generated by the limited AWG bandwidth dominates that due to the CD after the emulated 200-km fiber transmission, explaining the slight degradation of BER curves (w/o IQ imbalance compensation) compared to that in case 1.

Figure 9(b) shows an example of a 4-QAM constellation based on the raw data at a 10-dB OSNR. A large ISI, caused by the limited AWG bandwidth, is clearly visible. Without IQ imbalance compensation, the equalizer can effectively compensate for this ISI, as shown in Fig. 9(c). However, the BER is sharply degraded if the IQ imbalance is not compensated. Figures 9(d) and 9(e) present examples of constellations following compensation by the GSOP and BASS methods, respectively. Even though the IQ imbalance is compensated for, the constellation cannot be fully recovered; indeed, the samples' distributions change from circles to ellipses after IQ compensation, resulting in a penalty, as observed in Fig. 9. Note that the residual CFO makes the GSOP method less efficient than the BASS method.

In the next step, we validate our algorithm with 16-QAM signals with a 10° phase imbalance. The reported phase imbalance value is estimated based on the method in [23]. Figure 10(a) shows the measured BER evolution as a function of the OSNR in both cases 1 and 2. As for the 4-QAM signals, the B2B curve w/o IQ imbalance is first measured as a benchmark. Then, the IQ modulator phase bias is tuned to generate a 10° phase imbalance. In case 1, the OSNR penalty is 7 dB at a BER of 10^{-3} if the IQ imbalance is not compensated. Thanks to the compensation by the GSOP and BASS methods, the BER curves are brought back to the same level as the BER curve w/o IQ imbalance. Note that the 16-QAM signals are severely distorted by ISI due to the limited AWG bandwidth, as shown in Fig. 10(b) for an OSNR of 26 dB. The equalizer operates effectively to compensate for this ISI, even if the IQ imbalance is not compensated for, leading to a better constellation as demonstrated in Fig. 10(c) for a 26-dB OSNR. In case 2, where the effects of CFO and CD are applied to the measured raw data, the BER curve w/o IQ imbalance compensation is slightly degraded. As the order of the constellation is increased compared to the 4-QAM case, the effect of residual CFO on the operation of the other DSP stages becomes more important. More specifically, the GSOP decreases its performance, resulting in a 3-dB OSNR penalty at a BER of 10^{-3} compared to the case without CFO. Figure 10(d) presents an example of a 16-QAM constellation at an OSNR of 26 dB, compensated by the

TABLE II
COMPARISON OF HARDWARE COMPLEXITY[a]

Method	Real Additions	Real Multiplications	Square-Root Operators
GSOP	$4N-3$	$6N+4$	2
BASS	$13N$	$22N$	0

[a]N: total number of samples used for IQ imbalance compensation.

GSOP. The residual CFO has a reduced influence on the operation of the BASS method, with only a 1-dB OSNR penalty at a BER of 10^{-3}. Figure 10(e) shows a 16-QAM constellation for an OSNR of 26-dB, compensated by the BASS method, showing fewer dispersed constellation spots compared to those in Fig. 10(d). Note that our proposed BASS method can also contribute to the monitoring and diagnosis functions of the IQ imbalance by exploiting the asymptotic convergence values of the filter coefficients, as shown in [8]. Further discussion on these functions is out of the scope of this paper.

V. HARDWARE COMPLEXITY COMPARISON

To perform a fair comparison, only the IQ imbalance compensator complexity used on one polarization is compared between the GSOP and BASS methods, regardless of the complexity of the equalizer and other DSP blocks. It is assumed that the same total number of samples, N, is used for the different IQ imbalance compensators. Note that a multiplication between two complex numbers consists of 4 real multiplications and 2 real additions and that squaring a complex number needs 2 real multiplications and 1 real addition. Based on this analysis, Table II provides the summarized hardware complexities of the GSOP and BASS methods in terms of number of real additions, real multiplications, and square-root operators. It can be observed that the required total number of multiplications and additions of the GSOP method is nearly 3.5 times less than that of the BASS method. However, the BASS method does not require the square-root operator, as is the case in the GSOP method, bringing a simpler hardware implementation.

It should furthermore be noted that our proposed method operates at the sample rate, leading to a promising approach for parallel processing (which is preferable at the high bit rates used in optical transmission systems), whereas the GSOP method uses statistical calculations that can create a delay in parallel implementations.

VI. CONCLUSION

In this paper, we have studied and demonstrated a promising method for IQ imbalance compensation based on blind adaptive source separation in dual-polarization M-QAM optical coherent communication systems. The proposed method is numerically and experimentally validated with 10 Gbaud optical 4-QAM and 16-QAM signals subjected to 30° and 10° transmitter phase imbalance. The robustness of the proposed method is verified after 200-km optical fiber transmission and in the presence of residual carrier frequency offset. Compared to the Gram–Schmidt orthogonalization procedure, the BASS method outperforms the GSOP method regardless of the residual CFO. Although our proposed method requires more addition and multiplication operators compared to the GSOP, it can operate at the sample rate, which is highly suitable for parallel implementation.

ACKNOWLEDGMENT

This work was supported in part by the Contrat de Plan Etat-Région PONANT and the French Ministry of Research. We are grateful to the special issue editors, Prof. Walter Cerroni and Prof. Zabih Ghassemlooy, for the kind invitation of this paper submission. We also acknowledge the anonymous reviewers who enabled us to improve the paper. Portions of this work were presented at the IEEE International Conference on Communications in 2016 at the Optical Networks and Systems Symposium.

REFERENCES

[1] P. C. Schindler, D. Korn, C. Stamatiadis, M. F. O'Keefe, L. Stampoulidis, R. Schmogrow, P. Zakynthinos, R. Palmer, N. Cameron, Y. Zhou, R. G. Walker, E. Kehayas, S. Ben-Ezra, I. Tomkos, L. Zimmermann, K. Petermann, W. Freude, C. Koss, and J. Leuthold, "Monolithic GaAs electro-optic IQ modulator demonstrated at 150 Gbit/s with 64QAM," *J. Lightwave Technol.*, vol. 32, no. 4, pp. 760–765, Feb. 2014.

[2] I. Fatadin, S. J. Savory, and D. Ives, "Compensation of quadrature imbalance in an optical QPSK coherent receiver," *IEEE Photon. Technol. Lett.*, vol. 20, no. 20, pp. 1733–1735, Oct. 2008.

[3] R. Rios-Muller, J. Renaudier, and G. Charlet, "Blind receiver skew compensation and estimation for long-haul non-dispersion managed systems using adaptive equalizer," *J. Lightwave Technol.*, vol. 33, no. 7, pp. 1315–1318, Apr. 2015.

[4] M. S. Faruk and K. Kikuchi, "Compensation for in-phase/quadrature imbalance in coherent receiver front-end for optical quadrature amplitude modulation," *IEEE Photon. J.*, vol. 5, no. 2, 7800110, Apr. 2013.

[5] E. Porto da Silva and D. Zibar, "Widely linear equalization for IQ imbalance and skew compensation in optical coherent receivers," *J. Lightwave Technol.*, vol. 34, no. 15, pp. 3577–3586, Aug. 2016.

[6] T. Koike-Akino, D. S. Millar, K. Kojima, K. Parsons, T. Yoshida, K. Ishida, Y. Miyata, W. Matsumoto, and T. Mizuochi, "Turbo demodulation for LDPC-coded high-order QAM in presence of transmitter angular skew," in *Proc. European Conf. Optical Communication (ECOC)*, Cannes, France, 2014, paper Th.1.3.2.

[7] G. Khanna, S. Calabro, B. Spinnler, E. de Man, and N. Hanik, "Joint adaptive pre-compensation of transmitter I/Q skew and frequency response for high order modulation formats and high baud rates," in *Optical Fiber Communication Conf. (OFC)*, Los Angeles, 2015, paper M2G.4.

[8] C. R. S. Fludger and T. Kupfer, "Transmitter impairment mitigation and monitoring for high baud-rate, high order modulation systems," in *Proc. European Conf. Optical Communication (ECOC)*, Dusseldorf, Germany, 2016, pp. 256–258.

[9] T.-H. Nguyen, P. Scalart, M. Gay, L. Bramerie, C. Peucheret, T. Nguyen-Ti, M. Gautier, O. Sentieys, J.-C. Simon, and M. Joindot, "Blind adaptive transmitter IQ imbalance compensation in M-QAM optical coherent systems," in *Proc. IEEE Int. Conf. Communications (ICC)*, Kuala Lumpur, Malaysia, 2016, pp. 1643–1648.

[10] T.-H. Nguyen, M. Joindot, M. Gay, L. Bramerie, J.-C. Simon, P. Scalart, and O. Sentieys, "Carrier frequency offset estimation based on circular harmonic expansion for optical coherent M-QAM communication systems," in *Proc. Opto-Electronics and Communications Conf. (OECC)*, Shanghai, China, 2015, paper 15650013.

[11] T. Schenk, *RF Imperfections in High-Rate Wireless Systems*, 1st ed. The Netherlands: Springer, 2008, pp. 143–144.

[12] "Characteristics of Single-Mode Optical Fibre and Cable," ITU-T Recommendation G.652, Mar. 2003.

[13] S. J. Savory, "Digital filters for coherent optical receivers," *Opt. Express*, vol. 16, no. 2, pp. 804–817, Jan. 2008.

[14] F. N. Hauske, N. Stojanovic, C. Xie, and M. Chen, "Impact of optical channel distortions to digital timing recovery in digital coherent transmission systems," in *Proc. Int. Conf. Transparent Optical Networks (ICTON)*, Munich, Germany, 2010, paper We.D1.4.

[15] T.-H. Nguyen, P. Scalart, M. Gay, L. Bramerie, C. Peucheret, O. Sentieys, J.-C. Simon, and M. Joindot, "Bi-harmonic decomposition-based maximum log likelihood estimator for carrier phase estimation of coherent optical M-QAM," in *Optical Fiber Communication Conf. (OFC)*, Anaheim, 2016, paper Tu3K.3.

[16] R. Schmogrow, B. Nebendahl, M. Winter, A. Josten, D. Hillerkuss, S. Koenig, J. Meyer, M. Dreschmann, M. Huebner, C. Koos, J. Becker, W. Freude, and J. Leuthold, "Error vector magnitude as a performance measure for advanced modulation formats," *IEEE Photon. Technol. Lett.*, vol. 24, no. 1, pp. 61–63, Jan. 2012.

[17] S.-I. Amari and J.-F. Cardoso, "Blind source separation—Semiparametric statistical approach," *IEEE Trans. Signal Process.*, vol. 45, no. 11, pp. 2692–2700, Nov. 1997.

[18] J.-F. Cardoso and B. H. Laheld, "Equivariant adaptive source separation," *IEEE Trans. Signal Process.*, vol. 44, no. 12, pp. 3017–3030, Dec. 1996.

[19] M. Valkama, M. Renfors, and V. Koivunen, "Blind signal estimation in conjugate signal models with application to I/Q imbalance compensation," *IEEE Signal Process. Lett.*, vol. 12, no. 11, pp. 733–736, Nov. 2005.

[20] I. Fatadin, D. Ives, and S. J. Savory, "Blind equalization and carrier phase recovery in a 16-QAM optical coherent system," *J. Lightwave Technol.*, vol. 27, no. 15, pp. 3042–3049, Aug. 2009.

[21] T. Schmidl and D. Cox, "Robust frequency and timing synchronization for OFDM," *IEEE Trans. Commun.*, vol. 45, no. 12, pp. 1613–1621, Dec. 1997.

[22] T.-H. Nguyen, F. Gomez-Agis, M. Gay, L. Anet-Neto, P. Scalart, C. Peucheret, M. Joindot, O. Sentieys, J.-C. Simon, and L. Bramerie, "IQ imbalance compensation based on maximum SNR estimation in coherent QPSK systems," in *Proc. Int. Conf. Transparent Optical Networks (ICTON)*, Graz, Austria, 2014, paper Tu.C1.3.

[23] T.-H. Nguyen, P. Scalart, M. Joindot, M. Gay, L. Bramerie, C. Peucheret, A. Carer, J.-C. Simon, and O. Sentieys, "Joint simple blind IQ imbalance compensation and adaptive equalization for 16-QAM optical communications," in *Proc. Int. Conf. Communications (ICC)*, London, UK, 2015, pp. 4913–4918.